Analysis of a strike-slip fault network using high resolution multibeam bathymetry, offshore NW Devon U.K.

Casey W. Nixon[1], David J. Sanderson[1,2,3], Jonathan M. Bull[1]

[1] School of Ocean and Earth Science, University of Southampton, National Oceanography Centre Southampton, SO14 3ZH.

[2] School of Civil Engineering and the Environment, University of Southampton, SO17 1BJ.

[3] EPT, BP Exploration Operating Company Limited. Chertsey Road, Sunbury-on-Thames, TW16 7BP.

1. Introduction

The analysis of fault networks is vital to understanding the brittle deformation of the earths crust as faults rarely occur individually and without associated deformation. Therefore, the major aim of this paper is to assess the changes in geometry, fault displacement and topology within a strike-slip fault network at different scales, hence, investigating the role of small and large faults. It will also demonstrate the use of high resolution multibeam bathymetry data as a tool to map and analyse an offshore strike-slip fault network.

Initial work on fault populations includes the application of power-law distributions to fault populations. This has been particularly useful for describing fault growth by looking at the distribution of fault displacement and fault trace lengths (Cartwright et al., 1995; Gupta and Scholz, 2000; Soliva and Schultz, 2008; Xu et al., 2010). Geometric and kinematic studies of fault populations have also contributed by adding to the understanding of fault segmentation, growth and propagation (e.g. Peacock & Sanderson 1991, 1994; Cartwright et al., 1995; Childs et al., 2003; Taylor et al., 2004; Bull et al., 2006; Baudon and Cartwright, 2008). Other work has investigated the importance and contribution of small scale faulting to the overall extension of an area (e.g. Walsh et al., 1991; Marrett and Allmendinger, 1992, Putz-Perrier and Sanderson 2008a, 2010) and their role in block rotations (e.g. Peacock et al., 1998).

This work suggests that fault systems evolve by individual faults increasing in both length and displacement, and that they become more linked with increasing finite strain (Ferrill et al., 1999; Walsh et al., 2001). This has been further supported by studies which show that fault populations evolve into longer and simpler systems with strain becoming localized within a fault system (e.g. Cowie et al., 1995; Nicol et al., 1997; Cowie et al., 2005; Moriya et al., 2005; Soliva and Schultz, 2008).

The use of high resolution reflection seismology has helped investigate displacement rate patterns within fault networks, both temporally and spatially, adding further to our understanding of fault movement, interaction and linkage within fault networks (Taylor et al., 2004; Mouslopoulou et al., 2009; Nicol et al., 2010). More recently Nixon et al. (2011) use aerial photography combined with field data to map a strike-slip fault network at Westward Ho!, north Devon. This demonstrated a spatial variation in fault pattern, displacement distribution and kinematic behaviour, hence, illustrating the heterogeneity of deformation within a fault network.

This paper seeks to further this study by combining the techniques used in Nixon et al. (2011) with multibeam bathymetry data to map and describe a strike-slip fault network offshore Hartland Point, north Devon (Fig. 1). It will determine the overall fault trends and kinematic behaviour of the network, investigating the possible affects of changing resolution on the geometry, topology, connectivity, and strain distribution within the network. This is then compared and correlated with onshore strike-slip networks at Hartland Quay and Westward Ho!.

2. Geological Setting

The strike-slip faults in north Devon cut Upper Carboniferous mudstones, siltstones and sandstones of the Crackington, Westward Ho!, Bideford and Bude Formations (Fig. 1) (Higgs et al., 1990). These form part of the Culm Basin that was later inverted at the end of the Carboniferous period during Variscan deformation, which produced ~E-W trending upright folds throughout the region (Sanderson, 1979; 1984).

The strike-slip faults comprise NE-trending left-lateral faults and NW-trending right-lateral faults that are related to approximately N-S compression. The precise age of the strike-slip faults may not be determined stratigraphically, but field evidence shows that they do post-date the late Variscan folding (Higgs et al., 1990). Hence, it is thought that these faults formed in either: **1)** a late Variscan right-lateral shear zone that occured during the Late Paleozoic (Arthaud and Matte, 1977; Badham, 1982) caused by oblique NW-SE convergence between the African and European plates (Coward and McClay, 1983; Sanderson, 1984; Barnes and Andrews, 1986; Holdsworth, 1989); or **2)** during late Cretaceous-Tertiary N-S shortening (Lake and Karner, 1987; Chadwick, 1993; Peacock and Sanderson, 1998) caused by the northward collision of the African plate into the Eurasian plate and/or Atlantic ridge-push forces as Britain drifted from the American plate (Underhill and Patterson, 1998).

Some strike-slip faults in north Cornwall and Devon are known to be reactivated (Kim et al., 2001). For example, the Sticklepath-Lustleigh fault zone (Fig. 1) is thought to have formed in the late Variscan event as a NW-trending right-lateral fault zone before undergoing left-lateral reactivation in the late Cretaceous-Tertiary (Holloway and Chadwick, 1986). The faults at Hartland do not show signs of multiphase movement or reactivation and, hence, their precise age is not important for this study. What is important is that the upright folding, steeply dipping bedding and strike-slip nature of the faults allow accurate measurements of displacements from mapped offsets of folds and stratigraphy.

3. Mapping Methods

The strike-slip fault network was mapped from high resolution multibeam bathymetry data of the offshore region to the north and west of Hartland Point (Fig. 1). These data were collected as part of the UK Civil Hydrography Programme with the data being collected in 2007 and 2008 by two vessels: MV Meridian using a Reson 7125 400 kHz multibeam, and MV Jetstream using a Kongsberg Maritime EM3002D multibeam. The data are of high quality and image features at the coast in water depths of only –1.0 m chart datum. This coverage was achieved by surveying at high tide and utilising the large tidal range in the Bristol Channel.

The multibeam bathymetry data were imported into ArcGIS for analysis and interpretation, and a geo-referenced 3D image with a pixel resolution of 0.5 m was created. Interpretation was completed using Hillshade images which accentuated bedding and fault traces. The degree of slope was also calculated from the multibeam data, and this combined with measurement of the strike of identified bedding planes, allowed determination of the strike and dip of bedding.

The multibeam bathymetry (Fig. 2) revealed a submerged platform of bedrock extending ~2.5 km from the shore line which provided a much more extensive area of faulting to be mapped (~16 km^2), than that exposed at low tide on the wave-cut platforms. The high quality of the multibeam data allowed direct correlation of bedding and faults with features mapped onshore on wave-cut platforms (Fig. 2). However there are localised sand pockets offshore which prevents correlation in some of the more sheltered coves such as the areas between Dyers Lookout and Damehole Point and adjacent to Upright Cliff.

The faults were digitized along with cut-offs of marker beds that allowed the calculation of multiple, lateral separations along fault traces. Each fault was then segmented along its trace-length at each measured offset point and an average displacement determined for each fault segment. Offsets are difficult to measure at intersections between two faults, hence, fault segments that share an intersection point with another fault were attributed the same displacement value as the measured offset point at the other end of the segment. This means that all the faults comprising the network are divided into segments and that each is associated with a value of displacement. The extracted fault segment data was the primary structural data that was used for further analysis.

The mapped fault network was correlated with onshore field mapping at Hartland Quay (a well studied and easily accessible part of the coastline with numerous and well exposed fold hinge lines and faults), where further 3D structural data was collected including bedding, fault orientations and slickenside measurements where possible.

4. Mapping Results

4.1 Folds and bedding attitudes

The multibeam bathymetry images an extensive submerged platform of bedrock with a general E-W trend of moderately to steeply dipping and folded bedding. This matches the attitude of bedding seen in onshore cliffs and wave cut platforms (Fig. 3a). Onshore mapping from Hartland Quay shows that the bedding has been intensively folded, with chevron folds varying in wave-lengths from 15-80 m (Fig. 4). This folding has been studied in detail from the cliff outcrops (e.g. Tanner, 1992; Davison et al., 2004) and can also be seen offshore. Throughout the submerged platform many marker beds that can be traced around fold hinges (Fig. 3). Stereographic projections of poles to bedding show that the folds trend approximately E-W related to N-S compression (Fig. 5). The profile planes from both onshore and offshore bedding data correlate with each other (Fig. 5) indicating that the strike and dip measurements of bedding taken from the multibeam bathymetry data are accurate. However, there is a bias in the dip data from offshore due to the more limited availability of exposed bedding surfaces needed for slope calculations as the dip increases.

4.2 Relationship between faults and folding

Mapping from the multibeam bathymetry indicates there are two distinct sets of faults based on their trend and lateral separation. The NW-trending have consistent right-lateral separations and NE-trending faults have left-lateral separations (Fig. 2). The relationship between the mapped faults and folding indicates that the faults post-date the folding, as the faults cut and offset both layering and fold axial traces (Fig. 3b).

The fault sets mapped from the bathymetry can be traced onshore (Fig. 3c) and correlate with onshore observations at Hartland Quay, where there are many examples of NW-trending right-lateral faults and NE-trending left-lateral faults (Fig. 4). Folds at Hartland Quay are also cross-cut by the faults, with fold hinges defining piercement points on both fault sets that show a dominant component of strike-slip offset (Figs. 4 and 6). Furthermore, structural measurements taken from Hartland Quay show that the fault planes are sub-vertical and have sub-horizontal slickensides (Fig. 5a).

Thus, the mapped offshore and onshore faults are strike-slip based on the fact that:

1) They form two separate fault sets in map view that have consistent and opposite lateral separations, forming NW-trending right-lateral faults and NE-trending left-lateral faults (Fig. 2);
2) Both sets are steeply dipping with shallowly plunging slickensides (Fig. 5a);
3) They laterally offset fold hinges and limbs in the same direction (Figs. 3b and 4);

4) Fold hinge lines form piercement points with a dominant strike-slip displacement (Fig. 6a).

4.3 Spatial distribution and relative proportions of fault sets

The strike-slip fault network is dominated by NW-trending right-lateral faults as seen in the (length x displacement) weighted rose diagram (Fig. 2b). These make up 80% of the overall trace-length with the largest right-lateral faults showing displacements of up to 146 m. Left-lateral faults are less numerous and much smaller, forming conjugate intersections with right-lateral faults (Fig. 7).

The larger right-lateral faults have long traces (up to 2.6 km) that approximately divide the stratigraphy into elongated NW-trending blocks. Within these blocks are many smaller right-lateral and left-lateral faults. Many of these are isolated, but some are connected to each other by small left-lateral faults. Within the fault blocks there is a slight anticlockwise rotation of stratigraphy and, combined with the right-lateral dominance, this suggests that the strike-slip fault network is acting in a domino fashion controlled by the larger right-lateral faults (c.f. Nixon et al., 2011).

5. Displacement and Scaling

The ability to map displacements along the lengths of the fault traces allows the fault network to be displayed at different scales. Figure 8 shows a series of maps of the network produced by clipping the fault segments at different displacements, ranging from 0.5-50 m (Fig. 8). This is referred to as a ‘displacement cut-off’ and is similar to the approach used by Watterson et al. (1996) to analyse the scaling properties of faults in the South Yorkshire coalfield. Rather than giving a maximum displacement/throw to a whole fault trace this technique is applied to each fault segment, which provides a more accurate representation of resolution as it preserves the spatial location of the faults and clips trace lengths by removal of the low displacement segments at fault tips (c.f. Pickering et al. 1997).

Different attributes can be measured at each resolution clipping (i.e. trace-length, fault density, fault set percentages, strain etc.), which is particularly useful for analysing the distribution of each attribute across different sizes of fault within the network. Using 10 m as a displacement cut-off value allows a direct comparison of small and large fault segments and helps assess their role within the fault network, with small fault segments and large fault segments having <10 m displacement and >=10 m displacement, respectively. The value of 10 m is used as it corresponds with the approximate limit of resolution in many 3-D seismic reflection surveys.

5.1 Effects of scale on the spatial arrangement of the fault network

At high displacement cut-offs (i.e. Figs 8a and 8b) the network is dominated by a few, long, isolated right-lateral faults, but at lower cut-offs the system appears more connected with smaller conjugate left-lateral faults connecting the larger right-lateral faults (Figs 8c, d, and e). This is reflected in the trace-length percentages for each fault set with left-lateral faults increasing from 7% to 20% with the inclusion of faults with less than 10 m displacement (Fig. 9c).

The larger fault segments form boundaries to NW-trending elongated blocks of stratigraphy with small fault segments infilling the spaces in between, increasing fault density from 1.8 to 5.9 km^{-1} (1 km^{-1} represents 1 km of fault trace per square km). Consequently, at high displacement cut-offs coherent and “unfaulted” regions appear between a series of widely spaced right-lateral,faults when in reality there is deformation at a smaller scale within the blocks.

It is apparent that the small fault segments are either infilling faults, small left-lateral faults, or tips of larger faults. These are responsible for the increase in fault density and have a significant effect on the distribution of trace-length. A plot of trace-length density vs displacement cut-off (Fig. 9a) shows the distribution of fault trace-length across different fault sizes. The majority of trace-length is taken up by smaller fault segments with the larger-displacement (>10 m) fault segments only making up 30% of the trace-length. This is a further reflection of the increased deformation within the fault blocks with the inclusion of smaller fault segments.

There are few conjugate intersections between fault segments with >10 m displacement, with the formation of strike-slip relays (Peacock & Sanderson 1995) being the main source of fault interaction, whereas splays and abutting faults become more frequent with the inclusion of smaller fault segments. Hence, the fault network appears less connected at high displacement cut-offs.

This analysis shows that the spatial arrangement of the fault network varies with scale, with the appearance of left-lateral faults at higher resolutions. Watterson et al. (1996) observe a somewhat similar pattern for multiple sets of normal faults in the southern Yorkshire coal fields, with one fault set being cut out at high-throw cut-offs. This suggests that this variation with scale is common where one fault set is dominant.

5.2 Strain distribution

The displacements calculated for each fault segment were used in a tensor analysis of strain, which provides an estimate of the maximum extension and its orientation.

This involves the calculation of a Lagrangian strain tensor from the cross-product of the unit normal and displacement vectors of each fault segment. Peacock and Sanderson (1993) apply this to faults sampled along a line, using a weighting factor to correct for the orientation bias of such samples. The same approach is valid for sampling on a plane, where (displacement x segment length) / unit area replace the displacement / unit length in a line sample. The weight (w) is determined from the angle between the fault normal and the plane. As we are dealing with sub-vertical strike slip faults, both the fault normal and displacement vector lie close to the sub-horizontal plane of the sample and the weighting factor can be ignored (i.e. $w \rightarrow 1$). The eigenvectors and eigenvalues of the strain tensor provide estimates of the orientation and magnitude of the principal strains. For a more detailed methodology see Nixon et al. (2011).

The strain analysis shows that the area has an overall maximum extension of ~4.2% in a WNW-ESE orientation, with the large fault segments and small fault segments accommodating extensions of 3.5% and 0.7%, respectively (Table 1). The plot of percentage extension vs displacement cut-off shows the distribution of strain for different fault sizes within the network (Fig. 9b). Even though most of the fault trace length is taken up by smaller fault segments, 86% of the overall extension is accumulated on fault segments with >=10 m displacement and ~45% by fault segments with >40 m displacement.

There is a small variation in maximum horizontal extension direction from N113°E for large faults to N107°E for small faults (Table 1). Although small, and undoubtedly within the errors of the determination of the principal strain axes, this sense of rotation is consistent with the domino behaviour of the system. The overall orientation of maximum extension is N112°E (see Table 1) which is weighted more towards the large fault segments of the fault network. This indicates that the mechanical behaviour of the fault network is mainly controlled by the larger fault segments within the network.

Overall, the majority of strain throughout the strike-slip network is accommodated by the large fault segments. Putz-Perrier and Sanderson (2008) show similar distributions of strain for normal faults at Kimmeridge Bay with large faults accommodating 65% of the overall strain, suggesting localization of strain onto the larger faults. This has also been seen in numerical and physical modelling (Cowie et al., 1995; Ackermann et al., 2001; Mansfield and Cartwright, 2001).

Although strain is localized onto the larger fault segments, the smaller fault segments are still significant, accommodating 14% of the overall extension. This is due to the high trace-length of small fault segments. Thus, our work on strike-slip faults systems (this paper; Nixon et al*.,* 2011) supports similar work by Putz-Perrier & Sanderson (2008a,b, 2010) on normal faults, and establishes by direct measurement the relative contribution to deformation made by faults with different displacements. This is an important factor in understanding extension estimates from seismic data as the faults that are too small to be resolved seismically may contribute significantly to the total strain, as was originally suggested by extrapolation assuming power-law scaling (e.g. Walsh et al., 1991, Marrett and Allmindinger, 1992, Jackson and Sanderson 1992; Pickering et al., 1996).

Pickering et al. (1997) recognise that fault lengths and throws of normal fault tips are often not seismically resolved. Therefore, estimates of sub-seismic strain using displacement scaling of fault populations will still underestimate sub-seismic strain as they do not take into account any additional contribution from fault tips, linkage zones and associated damage. By using fault segments rather than individual faults, this study incorporates the effects of fault tips and linkage zones, with that of small faults, in evaluating their role in accommodating extension within a basin.

6. Topology

The fault network was analysed in terms of a system of fault branches between tips (I-nodes) or intersections (X- or Y-nodes) (Fig. 10). Manzocchi (2002) uses this system to estimate connectivity by looking at the relative proportions of I-, Y- and X-nodes for fracture networks. Like fracture networks, fault networks become connected through a combination of crossing fault intersections (X-nodes), and abutments and splays of fault tips (Y-nodes). Hence, for this study the combined percentage of X- and the Y-nodes was used to represent the connectivity of the fault network. This is then taken further by analysing how the percentage and nature of connecting nodes within the fault network changes with resolution.

The percentages of different node (Table 2) show that the fault network offshore Hartland Point is dominated by I-nodes (isolated tips). Connecting nodes make up just 21.2% of all nodes with the majority being Y-nodes. Two different types of Y-node can be identified: **1)** Synthetic Y-nodes where two faults with the same motion sense intersect resulting from a fault linkage or splay; and **2)** Antithetic Y-nodes where two faults with the opposite motion sense intersect as a result of one fault abutting another. The latter make up over 50% of all connecting nodes which emphasizes the importance of conjugate fault sets when considering the connectivity of a fault network.

The plot of connecting node % vs displacement cut-off shows that the percentage of fault branches ending at Y-shaped or X-shaped nodes approximately halves with the exclusion of the small fault segments (Fig. 11). This is quite significant considering that there are no connecting nodes present for fault segments at displacement cut-offs of greater than 25 m, resulting in the network appearing very unconnected at low resolutions. Furthermore, the nature of interacting Y- and X-nodes varies with scale. Synthetic Y-nodes (or splays) are dominant for faults with >5 m displacement, whereas for faults with <5 m displacement, antithetic Y-nodes dominate and crossing X-nodes are occasionally developed. This pattern suggests that larger faults are more likely to form linkage and splays, due to fault growth, and that low displacements are usually needed for crossing X-shaped fault intersections to be preserved.

Overall the offshore network at Hartland is poorly connected, but the connectivity of the strike-slip network increases with increasing resolution, particularly with the inclusion of faults smaller than the seismic resolution cut-off. This, combined with an increase in fault density from 1.8 to 5.9 km^{-1}, indicates that the connectivity of the fault network is very dependant on small fault segments. Pickering et al. (1997) found similar results when modeling the connectivity of normal fault tips, highlighting the importance of underestimating the connectivity of fault networks due to the limited resolution of seismic data.

7. Discussion and Comparison with Westward Ho!

Analysis of the offshore strike-slip fault network at Hartland shows that the distribution of different attributes varies with displacement. This has highlighted three main points: 1) small faults, fault tips and linkage zones contribute the majority of the overall trace-length; 2) strain is localized onto individual large displacement fault segments; 3) at low displacement cut-offs the fault network appears more connected with the inclusion of small faults, fault tips and linkage zones. To show that these observations are applicable to other fault networks, the same scaling analysis has been applied to an onshore strike-slip fault network at Westward Ho! previously described by Nixon et al. (2011).

7.1 Westward Ho!

The fault sets at Westward Ho! have orientations that match those found offshore from Hartland Point (NW-trending right-lateral faults and NE-trending left-lateral faults), and they also post-date folding. The network has large faults that divide the rock-mass into elongated blocks with small faults accommodating deformation within each block, not unlike the offshore network. There is much heterogeneity within the fault network at Westward Ho!, with fault set dominance changing throughout (Nixon et al., 2011), however the geometric and lithological similarities with the offshore fault network make Westward Ho! a good comparison. Three contrasting small areas of intense deformation from within the fault network at Westward Ho! were chosen for comparison (Fig. 12):

Left-lateral area – This has the highest strain value of the three areas with an overall maximum extension of ~26.8% and an orientation of N068°E resulting from the left-lateral dominance of the fault network (Nixon et al., 2011). The majority of the trace-length, 71%, is taken up by small fault segments (Table 1). However, 94% of the overall extension is accommodated by the larger fault segments, which is the largest proportion in comparison with the other two onshore areas.

Damage Area – This is a region of more internal deformation lying between large left-lateral faults (Fig. 12) and has an overall maximum extension of ~24.3% with an orientation of N077°E. The trace-length density is almost double the trace-length density of the left lateral area (Table 1) and small fault segments, make up 79% of overall trace-length (Table 1). Hence, the small fault segments are much more significant than in the left-lateral area and accommodate 14% of the overall extension.

Right-lateral area – This has the lowest strain value of the three areas with an overall maximum extension of ~15.7% and an orientation of N112°E. Again the majority of the trace-length is taken up by the small fault segments with only 12% being taken up by the large-fault segments (Table 1). The distribution of strain shows a similar pattern with 77% being localized onto the large fault segments, however, this is much less than both the left-lateral and damage areas (Table 1).

7.2 Strain

Overall the three areas at Westward Ho! accommodate much higher strains and fault densities in comparison with the offshore network at Hartland (Table 1). This is not an effect of resolution as it is consistent for all displacement cut-offs (Fig. 13), instead this indicates that the areas at Westward Ho! are more intensely deformed. The linear-log plots (Fig. 13) show that the three onshore areas have a similar pattern of trace-length and strain distribution to the fault network offshore. Most of the fault trace-length is taken up by small displacement (<10 m) fault segments and the majority of the strain is still accommodated by large displacement (>=10 m) fault segments, again supporting the idea of strain localization onto larger faults.

The distributions of strain for the three onshore areas at Westward Ho! show that more strain is localized onto the larger fault segments with an increase in strain (Table 1). This is reflected in the linear-log plot of strain vs displacement cut-off

(Fig. 13b) as an increase in gradient at higher displacements and suggests that as strain increases strain becomes localized onto higher displacement fault segments. This is consistent with the observations of Nicol et al. (1997) who show that, with increasing strain, networks have faults with higher displacement rates.

Whilst strain localization appears to increase with increasing strain for the three areas at Westward Ho!, the fault network offshore from Hartland Point does not fit this observation. Even though the offshore network accommodates much lower strains than the onshore areas at Westward Ho!, 85% of the strain is localized onto the large fault segments, which is a higher proportion than the right-lateral area and similar to the damage area (Table 1). This is due to the increased deformation seen at Westward Ho! as indicated by the high strains and fault densities (Table 1, Fig. 13). Strain is localized to areas of intense deformation, not just individual fault planes, and accommodated by internal deformation within fault blocks and associated damage zones. Hence, in areas of localized deformation less strain is localized on the larger fault segments due to increased amounts of internal deformation between large faults.

Pickering et al. (1996) found similar affects for normal faults by fitting to power-law distributions of the form

$$N \propto (\text{displacement})^{-D},$$

where the D-value is termed the power-law exponent. They found that for a D-value of 0.5 almost all the extension is taken up by faults with heaves greater than 20 m, whereas for a D-value of 0.9 their contribution decreases to less than half. As an increase in the D-value of a fault population reflects a higher degree of small-scale faulting, this supports the idea that for areas with increased amounts of internal deformation less strain is localized onto the larger faults.

The significance of small faults within areas of internal deformation is also reflected in the strain orientations with the damage area accommodating less rotation in comparison to the left-lateral area. This is opposite to the conclusions of Peacock et al. (1998) who proposed that small faults added to the overall rotation of an area. This difference is due to the nature of internal deformation, with the majority of small faults in this study being antithetic and conjugate to the bounding faults. Although the small fault segments have an increased significance in areas with increased deformation the majority of strain is still accommodated by the larger fault segments, indicating that the kinematic behaviour of the fault network is controlled by the large faults.

7.3 Connectivity

The connecting node percentage (X- and Y-nodes) for the left-lateral, damage and right-lateral areas at Westward Ho! are 45.5%, 73.5% and 37.5%, respectively (Table 2). The majority of connecting nodes are antithetic Y-nodes, which agrees with the offshore fault network and further emphasizes the importance of conjugate fault sets when considering connectivity. The percentages for all connecting nodes are much higher than the offshore network indicating that the three areas at Westward Ho! are better connected. The damage area is also the most connected, mainly due to its increased fault density.

A ternary plot of I-, Y-, and X-node proportions illustrates the connectivity changes of a fault network with increasing resolution. In general, the networks become better connected away from the I-node corner of the triangle (Fig. 14), but see

Manzocchi (2002) for a more detailed discussion of this in terms of percolation theory. Overall the proportion of connecting nodes within each fault network, from both Westward Ho! and Hartland Point, increases with increasing resolution. The right-lateral area has a similar connectivity pathway to the network at Hartland Point. They both follow the I-Y margin of the ternary diagram and only have a small contribution of connecting X-nodes, even at high resolutions. The left-lateral and damage areas also follow the I-Y line on the ternary diagram. However, they are influenced much more by the presence of connecting X-nodes and are more connected at higher resolutions.

All the fault networks experience a significant increase in the proportion of X- and Y-nodes once faults with less than 12 m displacement are included (Fig. 14). However, the fault networks at Westward Ho! are also better connected than at Hartland Point suggesting that fault networks become more connected with increasing strain (Table 2 and Fig.14). Furthermore, the damage area is much more connected than the right and left-lateral areas indicating that damage zones and areas with increased internal deformation are better connected. These areas often have increased numbers of smaller faults further supporting the idea that connectivity is reliant on small faults.

This indicates that even though the connectivity of fault networks is primarily dependant on the length, density and orientation of the faults and their spatial correlation (Berkowitz et al., 2000), strain and the nature of its localization also plays an important role. Fault networks appear to be better connected when strain is localized to an area, creating damage zones of intense deformation and high fault densities, rather than when strain is localized onto individual faults forming longer and simpler systems. This also suggests that connectivity increases with increased amounts of deformation. Micarelli et al. (2006) show similar results with the connectivity of fracture networks being higher in intensely deformed damage zones than in weakly deformed damage zones around normal fault planes.

8. Summary and Conclusions

Multibeam bathymetry has been used to identify and map an extensive area of a strike-slip fault network offshore from Hartland Point, north Devon. The fault network comprises NW trending right-lateral faults and NE trending left-lateral faults and behaves in a right-lateral domino fashion. The spatial arrangement, topology, and distribution of strain and trace-length of the fault network vary with resolution:

1) Small (<10 m) displacement fault segments infill fault blocks, bounded by large displacement (10-150 m) faults, and make up most of the trace-length.

2) Strain is localized onto the large-displacement fault segments with >=10 m displacement that bound the fault blocks.

3) The kinematic behaviour of the fault network is controlled by rotation between the large faults.

4) Fault networks appear less connected at lower resolutions as the connectivity of the fault network is very dependant on the presence of small fault segments.

Comparison with onshore field examples from Westward Ho! confirms these points with similar distributions of strain and fault trace-length. Furthermore, combining the two datasets suggests that strain localization and connectivity are influenced by both the overall strain and amount of internal deformation:

5. **5)** More strain is localized onto the larger-displacement fault segments, however, small fault segments can make an important contribution to strain in areas with large amounts of internal deformation (damage zones).

6. **6)** Connectivity of a fault network increases with increasing strain as well as with increasing resolution.

7. **7)** Damage zones and areas with internal deformation are better connected due to increased contributions of small fault segments and high fault densities.

8. **8)** Fault networks are better connected when strain is localized to an area rather than when strain is localized onto individual faults.

The comparison with the onshore fault networks at Westward Ho! confirms that the observations from the analysis of the offshore fault network at Hartland are applicable to other fault networks. The techniques and methods developed for this study have helped to further the analysis of fault networks. The application of high resolution multibeam bathymetry imagery has allowed expansion and uncovering of an extensive fault network. This combined with analysis of fault patterns, topology and distribution of resulting strains highlights the importance of resolution when investigating crustal deformation, particularly when considering faults smaller than the seismic resolution cut-off.

Acknowledgements

C.W. Nixon acknowledges financial support from NERC Case studentship (NE/H524922/1) with BP, and we are grateful to Steve Dee for his input into the project. We thank the United Kingdom Hydrographic Office for providing the multibeam bathymetry data (HI 1158: Bristol Channel - Barnstable Bay), and staff at the Maritime and Coastguard Agency in Southampton for useful discussions. Aerial photography was provided by the Channel Coastal Observatory.

References

Ackermann, R.V., Schlische, R.W., Withjack, M.O., 2001. The geometric and statistical evolution of normal fault systems: and experimental study of the effects of mechanical layer thickness on scaling laws. Journal of Structural Geology 23, 1803-1326.

Arthaud, F., Matte, P., 1977. Late Paleozoic strike-slip faulting in southern Europe and northern Africa: Result of a right-lateral shear-zone between the Appalachians and the Urals. Geological Society of America Bulletin 88, 1305-1320.

Badham, J.P.N., 1982. Strike-slip orogens – an explanation for the Hercynides. Journal of the Geological Society 139, 493-504.

Barnes, R.P., Andrews, J.R., 1986. Upper Palaeozoic ophiolite generation and obduction in south Cornwall. Journal of the Geological Society 143, 117-124.

Berkowitz, B., Bour, O., Davy, P., Odling, N., 2000. Scaling of fracture connectivity in geological formations. Geophysical Research Letters 37, 2061-2064.

Bull, J.M., Barnes, P.M., Lamarche, G., Sanderson, D.J., Cowie, P.A., Taylor, S.K., Dix, D.K., 2006. High-resolution record of displacement accumulation on an active normal fault: implications for models of slip accumulation during repeated earthquakes. Journal of Structural Geology 28, 1146-1166.

Cartwright, J.A., Trudgill, B.D., Mansfield, C.B., 1995. Fault growth by segment linkage: an explanation for scatter in maximum displacement and trace length data from the Canyonlands Grabens of SE Utah. Journal of Structural Geology 17, 1319-1326.

Chadwick, R.A., 1993. Aspects of basin inversion in southern Britain. Journal Geological Society of London 150, 311-322.

Childs, C., Nicol, A., Walsh, J.J., Watterson, J., 2003. The growth and propagation of synsedimentary faults. Journal of Structural Geology 25, 633-648.

Coward, M.P., McClay, K.R., 1983. Thrust tectonics of S.Devon. Journal Geological Society of London 140, 215-228.

Cowie, P.A., Sornette, D.C., Vanneste, C., 1995. Multifractal scaling properties of a growing fault population. Geophysical Journal International 122, 457-469.

Cowie, P.A., Underhill, J.R., Behn, M.D., Lin, J., Gill, C.E., 2005. Spatio-temporal evolution of strain accumulation derived from multi-scale observations of Late Jurassic rifting in the northern North Sea: A critical test of models for lithospheric extension. Earth and Planetary Science Letter 234, 401-419.

Davison, I., Jeffcoate, A., Qing, H., 2004. Geometry of chevron folding and shortening estimates at Hartland Quay, North Cornwall, UK, and some regional implications for Culm Basin development. Geoscience in south-west England 11, 42-50.

Ferrill, D.A., Stamatakos, J.A., Sims, D., 1999. Normal fault corrugation: implications for growth and seismicity of active normal faults. Journal of Structural Geology 21, 1107-1110.

Gupta, A., Scholz, C.H., 2000. Brittle strain regime transition in the Afar depression: Implications for fault growth and seafloor spreading. Geology 28, 1087-1090.

Higgs, R., Reading, H.G., Li, X., 1990. Upper Carboniferous lacustrine and deltaic sedimentology, SW England: Westward Ho! and Bude. British Sedimetological Research Group.

Holdsworth, R.E., 1989. The Start-Perranporth line: a Devonian terran boundary in the Variscan orogen on SW England. Journal Geological Society of London 146, 419-421.

Holloway, S., Chadwick, R.A., 1986. The Sticklepath-Lustleigh fault zone: Tertiary sinistral reactivation of a Variscan dextral strike-slip fault. Journal Geological Society of London 143, 447-452.

Jackson, P., Sanderson, D.J., 1992. Scaling of fault displacements from the Badojoz – Cordoba shear zone, SW Spain. Tectonophysics 210, 179-190.

Kim, Y.-S., Andrews, J.R., Sanderson, D.J., 2001. Reactivated strike-slip faults: examples from north Cornwall. Tectonphysics 340, 173-194.

Lake, S.D., Karner, G.D., 1987. The structure and evolution of the Wessex Basin, southern England: an example of inversion tectonics. Tectonophysics 137, 347-378.

Mansfield, C., Cartwright, J., 2001. Fault growth by linkage: observations and implications from analogue models. Journal of Structural Geology 23, 745-763.

Manzocchi, T., 2002. The connectivity of two-dimensional networks of spatially correlated fractures. Water Resources Research 38, 1162, doi:10.1029/2000WR000180.

Marrett, R., Allmendinger, R.W., 1992. Amount of extension on “small” faults: An example from the Viking graben. Geology 20, 47-50.

Micarelli, L., Benedicto, A., Wibberley, C.A.J., 2006. Structural evolution and permeability of normal fault zones in highly porous carbonate rocks. Journal of Structural Geology 28, 1214-1227.

Moriya, S., Childs, C., Manzocchi, T., Walsh, J.J., 2005. Analysis of the relationships between strain, polarity and population slope for normal fault systems. Journal of Structural Geology 27, 1113-1127.

Mouslopoulou, V., Walsh, J.J., Nicol, A., 2009. Fault displacement rates on a range of timescales. Earth and Planetary Science Letters 278, 186-197.

Nicol, A., Walsh, J.J., Watterson, J., Underhill, J.R., 1997. Displacement rates of normal faults. Nature 390, 157-159.

Nicol, A., Walsh, J.J., Villamor, P., Seebeck, H., Berryman, K.R., 2010. Normal fault interactions, paleoearthquakes and growth in an active rift. Journal of Structural Geology 32, 1101-1113.

Nixon, C.W., Sanderson, D.J., Bull, J.M., 2011. Deformation within a strike-slip fault network at Westward Ho!, Devon U.K.: Domino vs conjugate faulting. Journal of Structural Geology 33, 833-843.

Peacock, D.C.P., 1991. Displacements and segment linkage in strike-slip fault zones. Journal of Structural Geology 13, 1025-1035.

Peacock, D.C.P., Sanderson, D.J., 1993. Estimating strain from fault slip using a line sample. Journal of Structural Geology 15, 1513-1516.

Peacock, D.C.P., Sanderson, D.J., 1994. Geometry and development of relay ramps in normal fault systems. American Association of Petroleum Geologists Bulletin 78, 147-165.

Peacock, D.C.P., Sanderson, D.J., 1995. Strike-slip relay ramps. Journal of Structural Geology 17, 1351-1360.

Peacock, D.C.P., Sanderson, D.J., 1998. Deformation history and basin-controlling faults in the Mesozoic sedimentary rocks of the Somerset coast. Proceedings Geological Association 110, 41-52.

Peacock, D.C.P., Anderson, M.W., Morris, A., Randall, D.E., 1998. Evidence for the importance of 'small' faults on block rotation. Tectonophysics 299, 1-13.

Pickering, G., Bull, J.M., Sanderson, D.J., 1996. Scaling of fault displacements and implications for the estimation of sub-seismic strain, in Buchanan, P.G., Nieuwland, D.A. (Eds), Modern developments in structural interpretation, validation and modelling. Geological Society London Special Publications 99, 11-26.

Pickering, G., Peacock, D.C.P., Sanderson, D.J., Bull, J.M., 1997. Modeling tip zones to predict the throw and length characteristics of faults. American Association of Petroleum Geologists Bulletin 81, 82-99.

Putz-Perrier, M.W., Sanderson, D.J., 2008a. The distribution of faults and fractures and their importance in accommodating extensional strain at Kimmeridge Bay, Dorset, UK. Geological Society London Special Publication 299, 97-111.

Putz-Perrier, M.W., Sanderson, D.J., 2008b. Spatial distribution of brittle strain in layered sequences. Journal of Structural Geology 30, 50-64.

Putz-Perrier, M.W., Sanderson, D.J., 2010. Distribution of faults and extensional strain in fractured carbonates of the North Malta Graben. American Association of Petroleum Geologists Bulletin 94, 435-456.

Sanderson, D.J., 1979. The transition from upright to recumbent folding in the Variscan fold belt of southwest England: a model based on the kinematics of simple shear. Journal of Structural Geology 1, 171-180.

Sanderson, D.J., 1984. Structural variation across the northern margin of the Variscides in NW Europe. Journal Geological Society of London Special Publications 14, 149-165.

Soliva, R., Schultz, R.A., 2008. Distributed and localized faulting in extensional settings: Insight from the North African Rift – Afar transition area. Tectonics 27, TC2003, doi:10.1029/2007TC002148.

Tanner, G.W.P., 1992. Morphology and geometry of duplexes formed during flexural-slip folding. Journal of Structural Geology 14, 1173-1192.

Taylor, S.K., Bull, J.M., Lamarche, G., Barnes, P.M., 2004. Normal fault growth and linkage in the Whakatane Graben, New Zealand, during the last 1.3 Myr. Journal of Geophysical Research 109, B02408.

Underhill, J.R., Paterson, S., 1998. Genesis of tectonic inversion structures: seismic evidence for the development of key structures along the Purbeck – Isle of Wright Disturbance. Journal of the Geological Society 155, 975-992.

Walsh, J.J., Watterson, J., Yielding, G., 1991. The importance of small scale faulting in regional extension. Nature 351, 391-393.

Walsh, J.J., Childs, C., Manzocchi, T., Imber, J., Nicol, A., Meyer, V., Tuckwell, G., Bailey, W.R., Bonson, C.G., Watterson, J., Nell, P.A.R., Strand, J., 2001.

Geometrical controls on the evolution of normal fault systems, in Holdsworth, R.E. (Ed.), The nature of the tectonic significance of fault zone weakening: Geological Society London Special Publication 186, 157–170.

Watterson, J., Walsh, J.J., Gillespie, P.A., Easton, S., 1996. Scaling systematics of fault sizes on a large-scale range fault map. Journal of Structural Geology 18, 199-214.

Xu, S., Nieto-Samaniego, A.F., Alaniz-Alvarez, S.A., Velasquillo-Martinez, L.G., Grajales-Nishimura, J.M., Garcia-Hernandez, J., Murillo-Muneton, G., 2010. Changes in fault length distribution due to fault linkage. Journal of Geodynamics 49, 24-30.

Figure Captions

Fig. 1 Location map with the main geological units. The grey area represents the interpreted offshore region.

Fig. 2 a) Interpreted multibeam bathymetry image from offshore Hartland Point showing the extent of the mapped fault network. Inset are the locations of the images in Fig. 3. b) Length-weighted rose diagram indicating the main fault trends.

Fig. 3 Multibeam bathymetry images with applied hillshade effect showing the quality of the imagery and the onshore-offshore correlation: a) An aerial photograph image (onshore) of strata and fold structures (grey) that can be traced into the offshore bathymetry survey (colour); b) An image of the sea-bed c. 2.5 km offshore showing an anticline that is cut by right and left-lateral faults showing offsets in the same direction on both limbs; c) An offshore bathymetry image (colour) with faults, strata and foldstructures which can be traced onto an onshore aerial photograph (grey).

Fig. 4 Fault map of a wave-cut platform at Hartland Quay showing lateral offsets of fold axial traces. Points A-A’ and B-B’ represent the piercement points shown in the field photographs in Figure 6a and b, respectively.

Fig. 5 Equal-area stereographic projections: a) fault and bed data from Hartland Quay, the dotted lines represent right-lateral faults and solid lines represent left-lateral faults; b) offshore bedding data measured from the multibeam bathymetry.

Fig. 6 Interpretation of field photographs from Hartland Quay showing folds cut by strike-slip faults, a) Small fold with steeper N-dipping and shallower S-dipping limb, with hinge in same bed forming a piercement offset of 8.4 m right-laterally (A-A’). b) Large fold with hinge in same bed offset ~48 m right-laterally (B-B’).

Fig. 7 A plot of displacement against azimuth for the fault segment data offshore from Hartland Point.

Fig. 8 Displacement maps of fault segments offshore Hartland Point. Each map has a different displacement cut-off representing different resolutions: a) 50 m, b) 20 m, c) 10 m, d) 3 m and e) 0.5 m.

Fig. 9 Linear-log plots of fault data from offshore Hartland Point showing the distribution of trace-length (a) and % extension (b) vs displacement cut-off. c)

Indicates the proportion of trace-length taken up by right-lateral (black) and left-lateral (grey) faults.

Fig. 10 a) Schematic diagram illustrating a system with fault branches and nodes. b) A ternary plot of I-, Y-, and X-node proportions illustrating the connectivity of the schematic fault network. In general, fault networks become better connected away from the I-node corner of the triangle, see Manzocchi (2002) for a more detailed discussion of this in terms of percolation theory.

Fig. 11 Linear-log plot of connecting node % vs displacement cut-off.

Fig. 12 Fault map of the wave-cut platform at Westward Ho! showing the localities of the left-lateral, damage and right-lateral areas, respectively. Modified from Nixon et al. (2011).

Fig. 13 Linear-log plots of fault data from the left-lateral, damage and right-lateral areas. a) trace-length density vs displacement cut-off and b) % extension vs displacement cut-off. The data for the offshore network is also included for comparison (grey).

Fig. 14 Ternary diagram of I-, Y- and X-Node percentages showing the connectivity pathways from 50 m resolution to full resolution of the fault networks from offshore Hartland Point and onshore Westward Ho!.

Table
Click here to download Table: Table 1.doc

Table 1. Structural characteristics and distribution of strain and trace-length within the fault networks offshore Hartland Point and onshore Westward Ho!

	Offshore Hartland Point			Left-lateral - Westward Ho!			Damage - Westward Ho!			Right-lateral - Westward Ho!		
	Overall	Small fault segments (<10 m)	Large fault segments (>=10 m)	Overall	Small fault segments (<10 m)	Large fault segments (>=10 m)	Overall	Small fault segments (<10 m)	Large fault segments (>=10 m)	Overall	Small fault segments (<10 m)	Large fault segments (>=10 m)
Trace-length	-	70%	30%	-	71%	29%	-	79%	21%	-	88%	12%
% extension	4.2	0.7	3.5	26.8	1.6	25.2	24.3	3.4	20.8	15.7	3.5	12.2
Proportion of Strain	-	14%	86%	-	6%	94%	-	14%	86%	-	23%	77%
Orientation of maximum extension (θ)	N112°E	N107°E	N113°E	N068°E	N089°E	N067°E	N077°E	N093°E	N074°E	N112°E	N107°E	N114°E
Fault Density (km^{-1})	5.9	-	-	39.5	-	-	80.4	-	-	45.1	-	-

Table 2. Nodal percentages of the fault networks from offshore Hartland Point and onshore Westward Ho!

	I-Node %	Y-Node %		X-Node %
		Synthetic	Antithetic	
Offshore Hartland Point	78.8	6.5	11.5	3.2
Left-lateral - Westward Ho!	54.5	6.4	25.7	13.4
Damage - Westward Ho!	26.5	18.8	42.7	12.0
Right-lateral - Westward Ho!	63.5	15.2	19.2	2.1

Figure

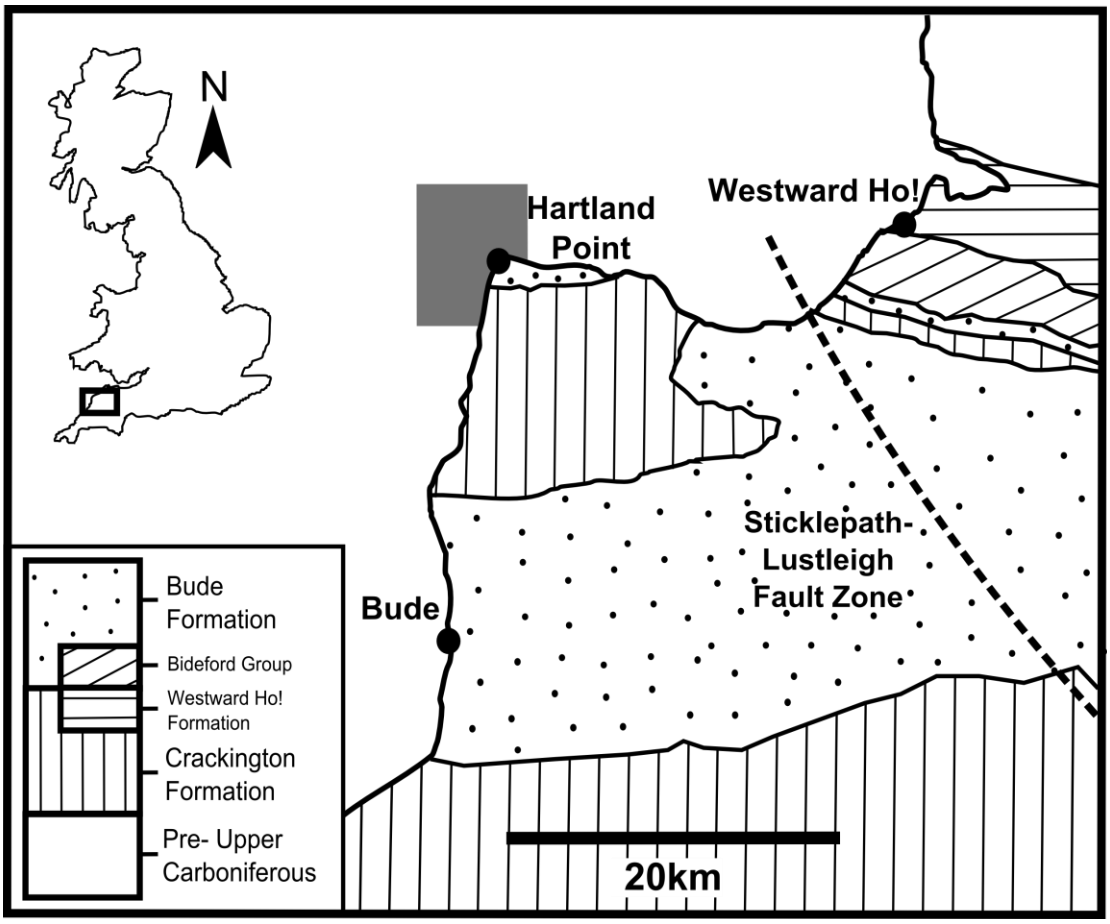
N
Hartland
Point
Westward Ho!
Sticklepath-
Lustleigh
Fault Zone
Bude
20km
Bude
Formation
Bideford Group
Westward Ho!
Formation
Crackington
Formation
Pre- Upper
Carboniferous

Figure

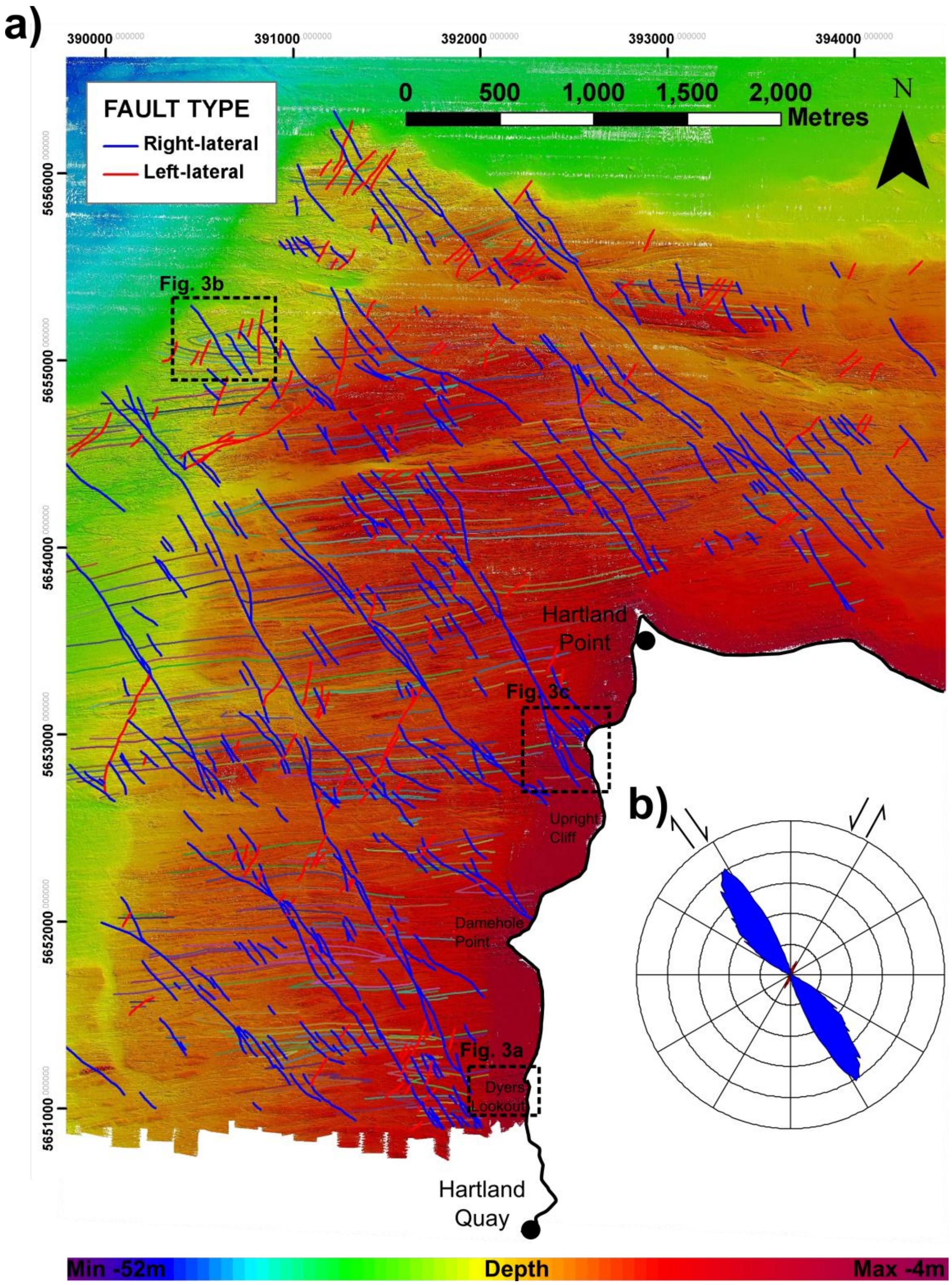
a)
390000
391000
392000
393000
394000
5656000
5655000
5654000
5653000
5652000
5651000
FAULT TYPE
Right-lateral
Left-lateral
0 500 1,000 1,500 2,000
Metres
N
Fig. 3b
Fig. 3c
Fig. 3a
Hartland Point
Upright Cliff
Damehole Point
Dyers Lookout
Hartland Quay
b)
Min -52m
Depth
Max -4m

Figure

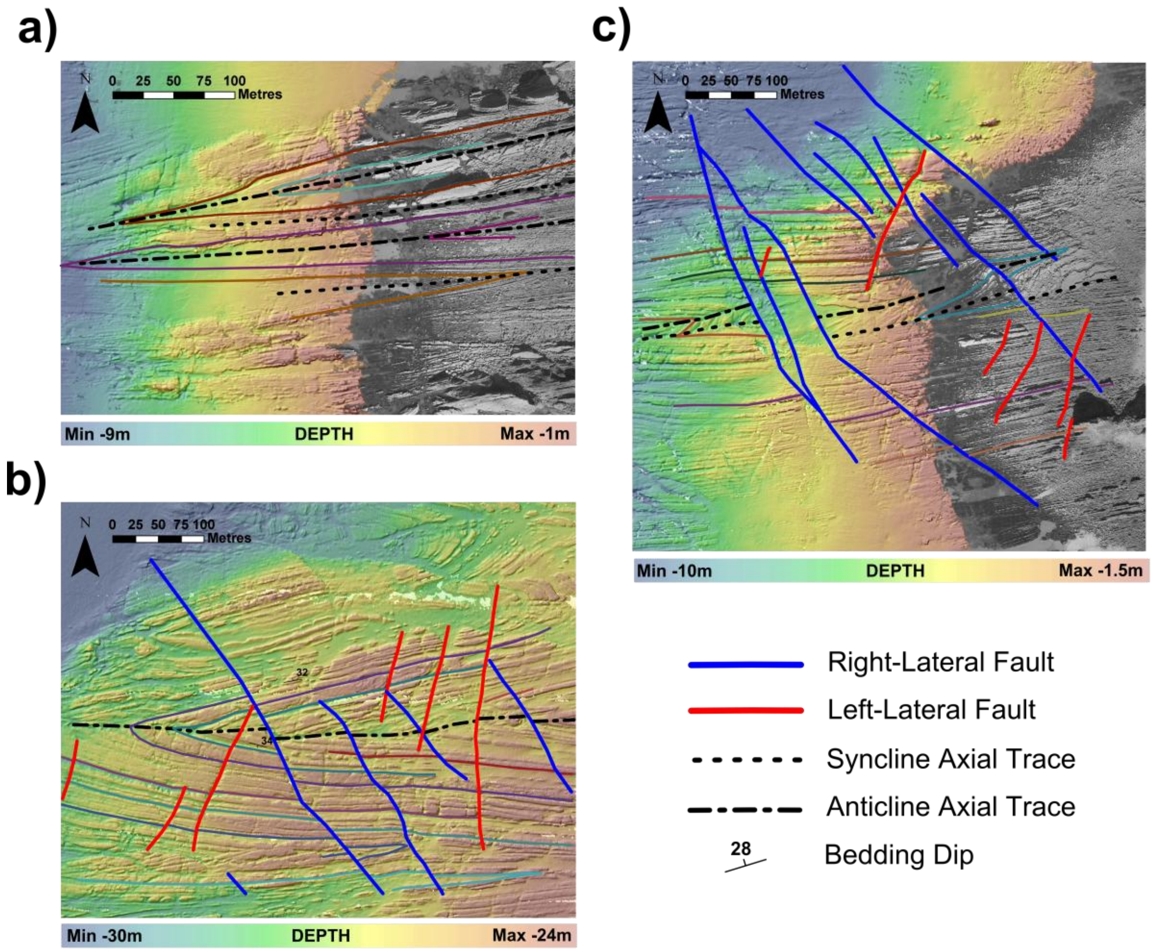

a)
N
0 25 50 75 100
Metres
Min -9m
DEPTH
Max -1m
b)
N
0 25 50 75 100
Metres
32
34
Min -30m
DEPTH
Max -24m
c)
N
0 25 50 75 100
Metres
Min -10m
DEPTH
Max -1.5m
Right-Lateral Fault
Left-Lateral Fault
Syncline Axial Trace
Anticline Axial Trace
28
Bedding Dip

Figure

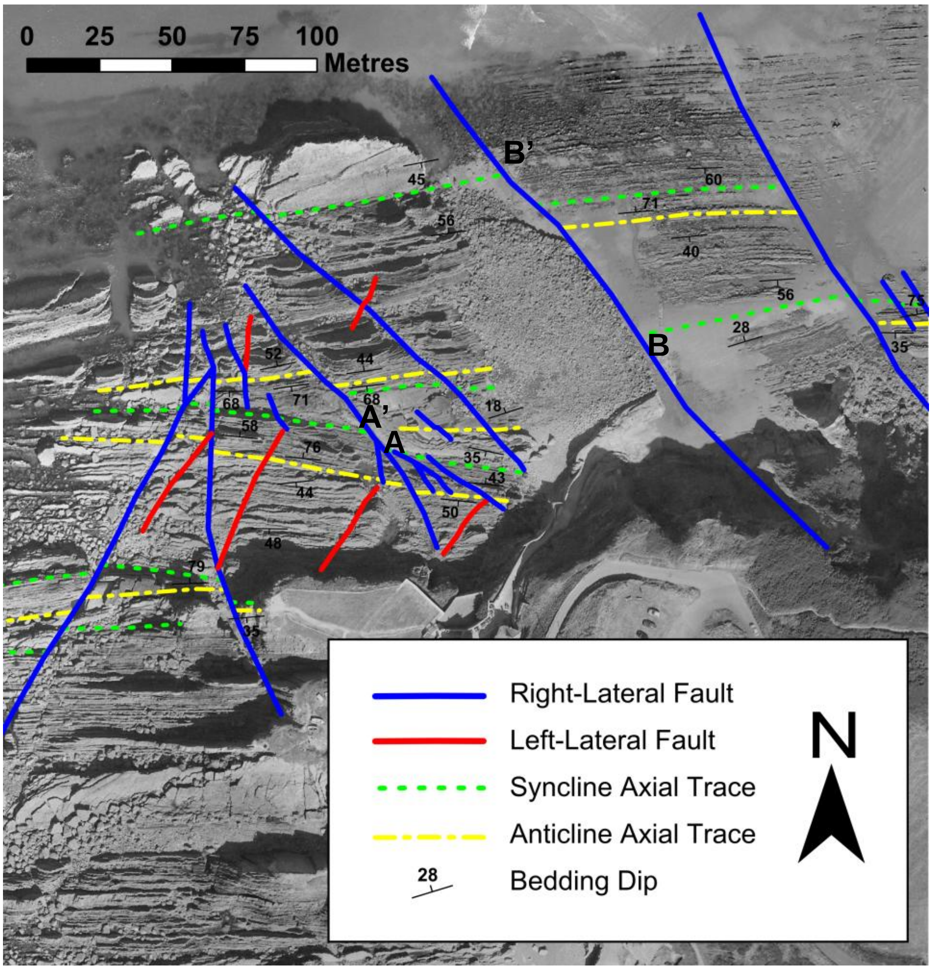
0 25 50 75 100
Metres
B'
B
A'
A
45
56
60
71
40
56
28
73
35
52
44
68
71
68
58
18
76
35
43
44
50
48
79
35
Right-Lateral Fault
Left-Lateral Fault
Syncline Axial Trace
Anticline Axial Trace
28
Bedding Dip
N

Figure

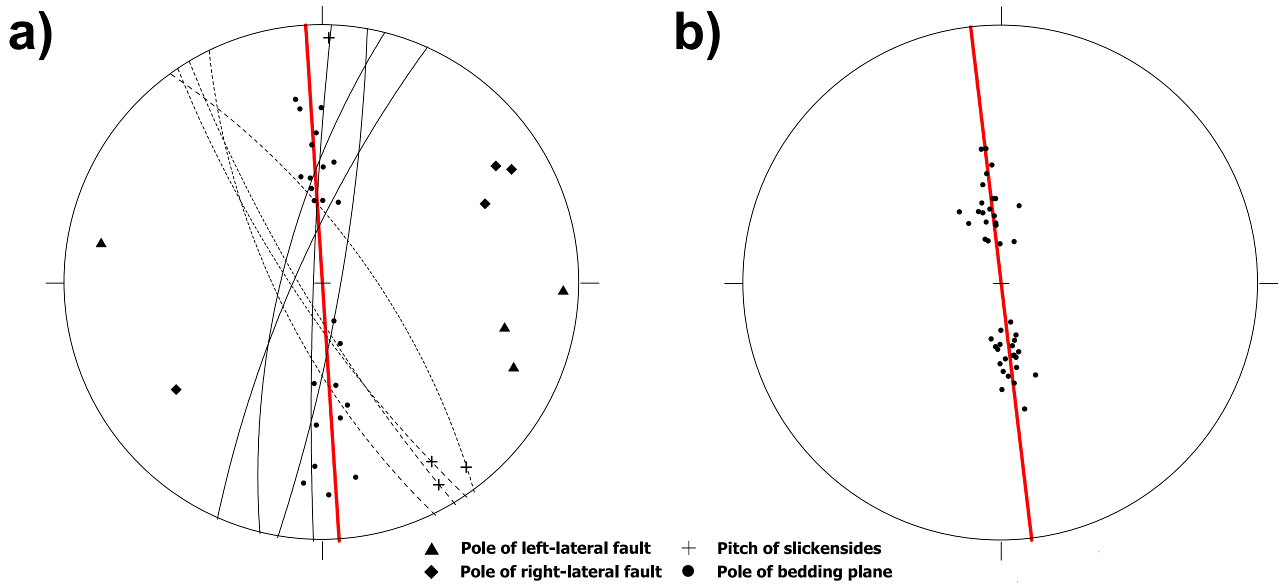
a)
b)
Pole of left-lateral fault
Pole of right-lateral fault
Pitch of slickensides
Pole of bedding plane

Figure

a)

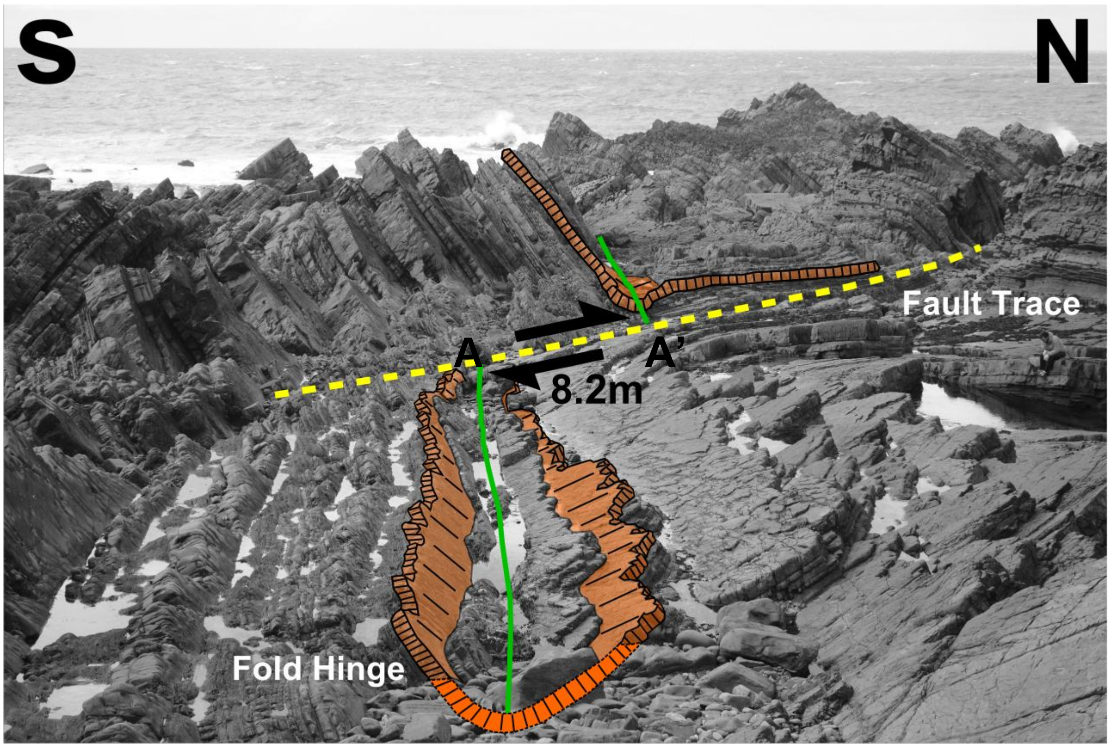
S
N
Fault Trace
A
A'
8.2m
Fold Hinge

b)

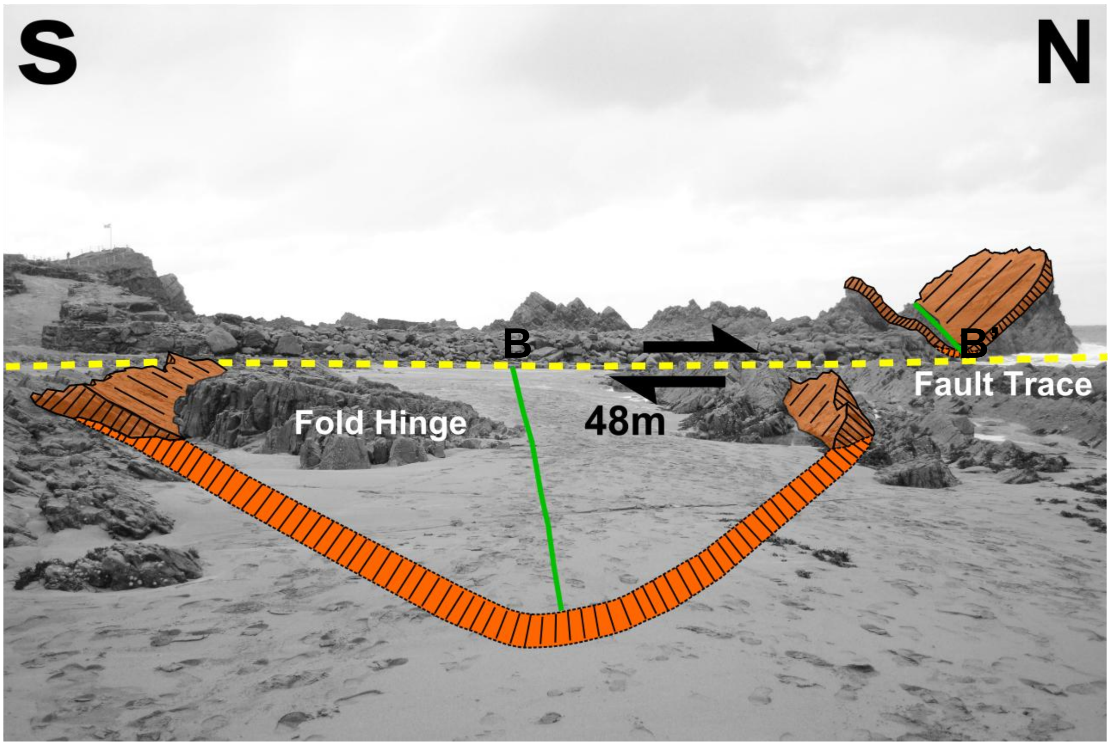
S
N
B
B'
Fault Trace
Fold Hinge
48m

Figure

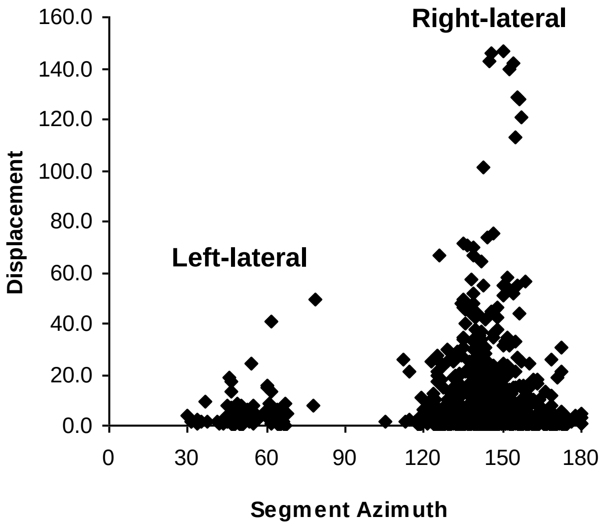

Right-lateral
Left-lateral
Displacement
160.0
140.0
120.0
100.0
80.0
60.0
40.0
20.0
0.0
0
30
60
90
120
150
180
Segment Azimuth

Figure

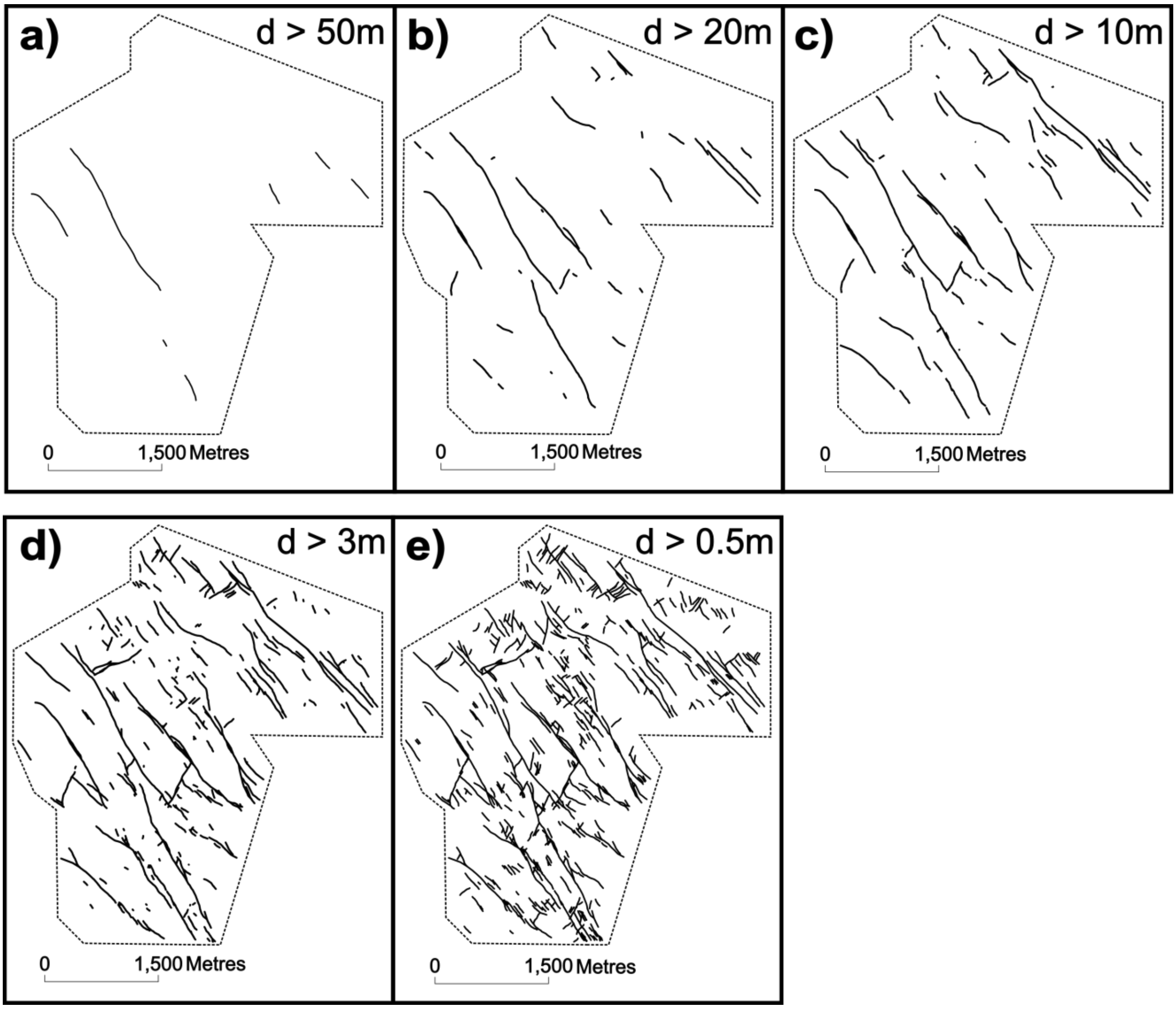

a)
d > 50m
0
1,500 Metres
b)
d > 20m
0
1,500 Metres
c)
d > 10m
0
1,500 Metres
d)
d > 3m
0
1,500 Metres
e)
d > 0.5m
0
1,500 Metres

Figure

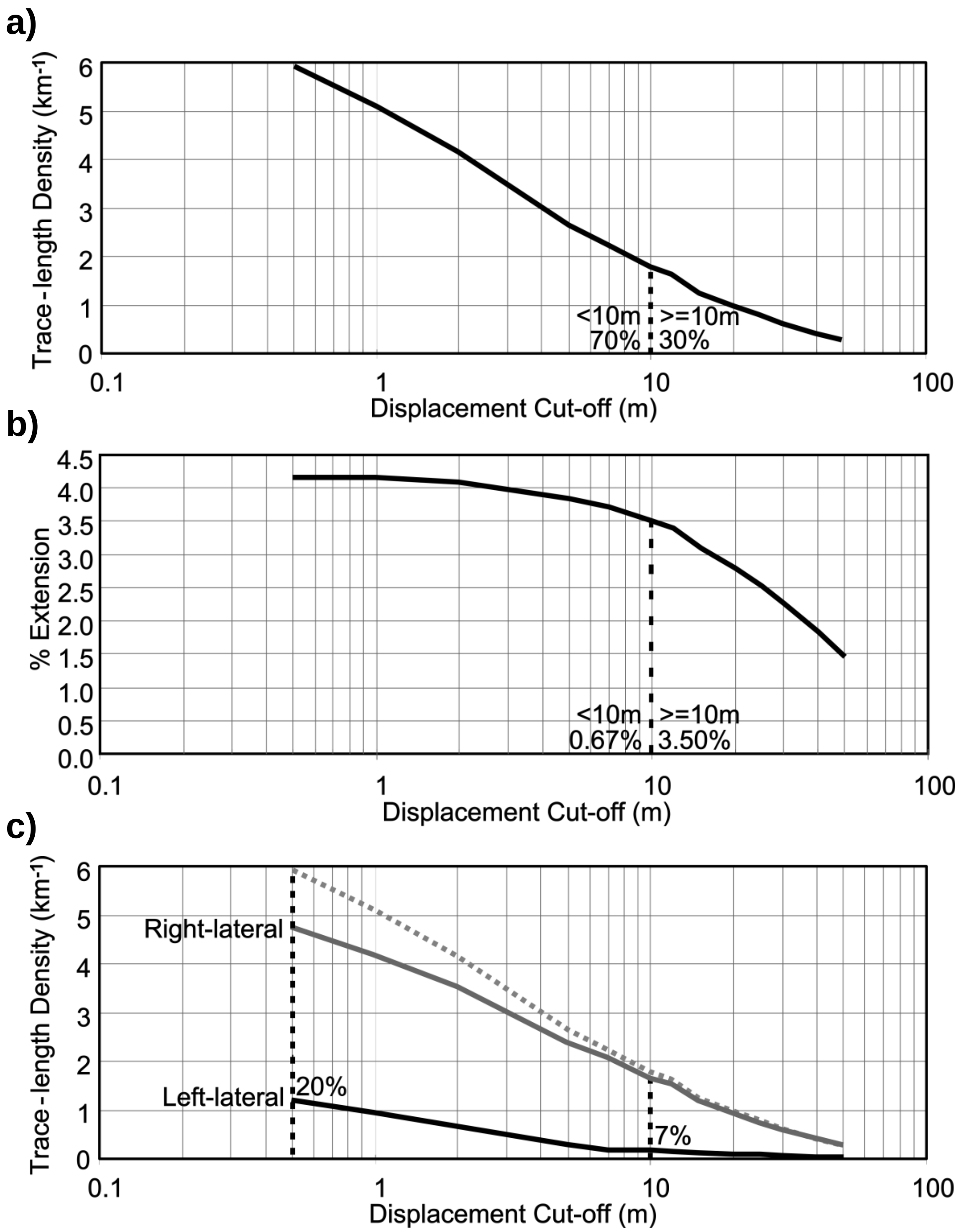
a)
Trace-length Density (km-1)
6
5
4
3
2
1
0
<10m
70%
>=10m
30%
0.1
1
10
100
Displacement Cut-off (m)
b)
% Extension
4.5
4.0
3.5
3.0
2.5
2.0
1.5
1.0
0.5
0.0
<10m
0.67%
>=10m
3.50%
0.1
1
10
100
Displacement Cut-off (m)
c)
Trace-length Density (km-1)
6
5
4
3
2
1
0
Right-lateral
Left-lateral
20%
7%
0.1
1
10
100
Displacement Cut-off (m)

Figure

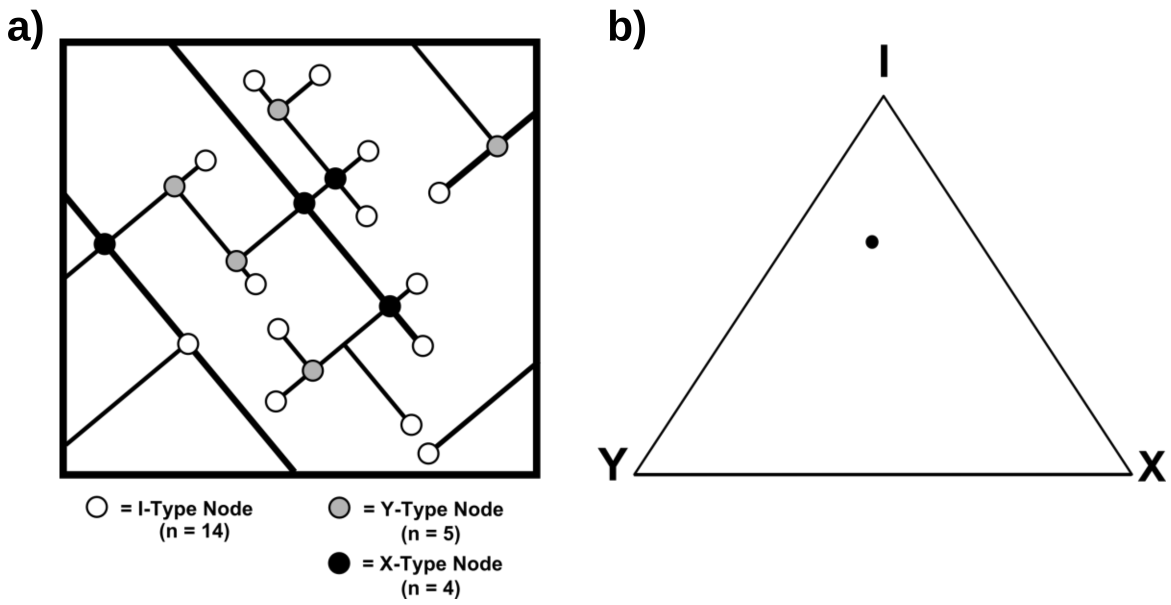

Figure

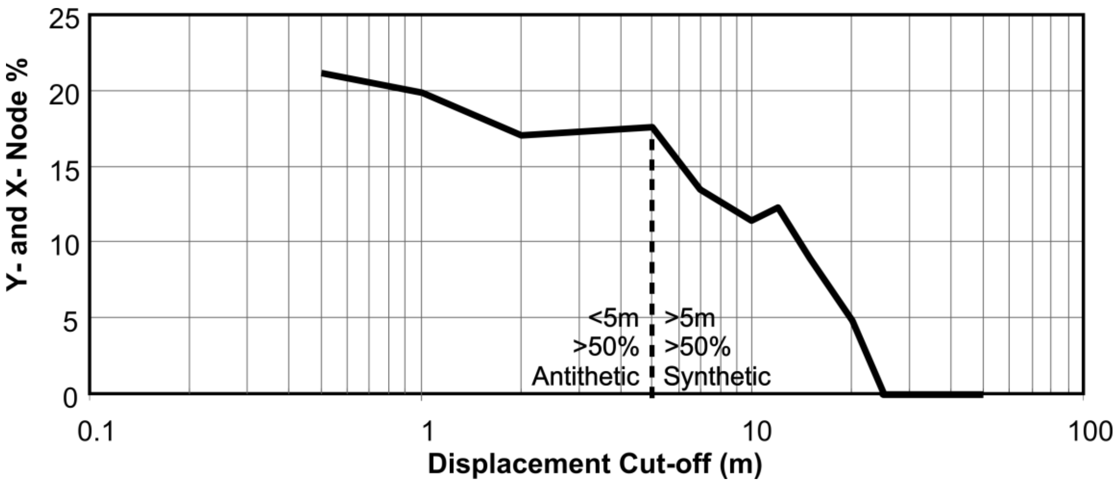

25
20
15
10
5
0
Y- and X- Node %
0.1
1
10
100
Displacement Cut-off (m)
<5m
>50%
Antithetic
>5m
>50%
Synthetic

Figure

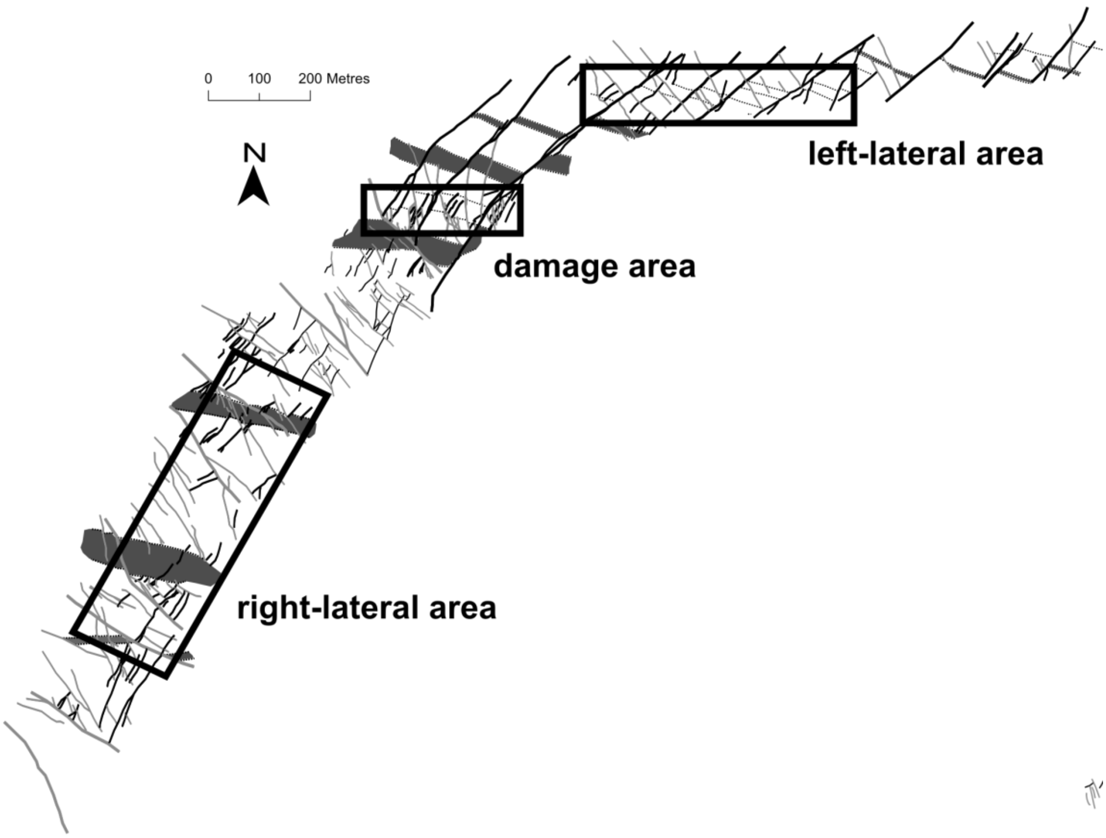
0 100 200 Metres
N
left-lateral area
damage area
right-lateral area

Figure

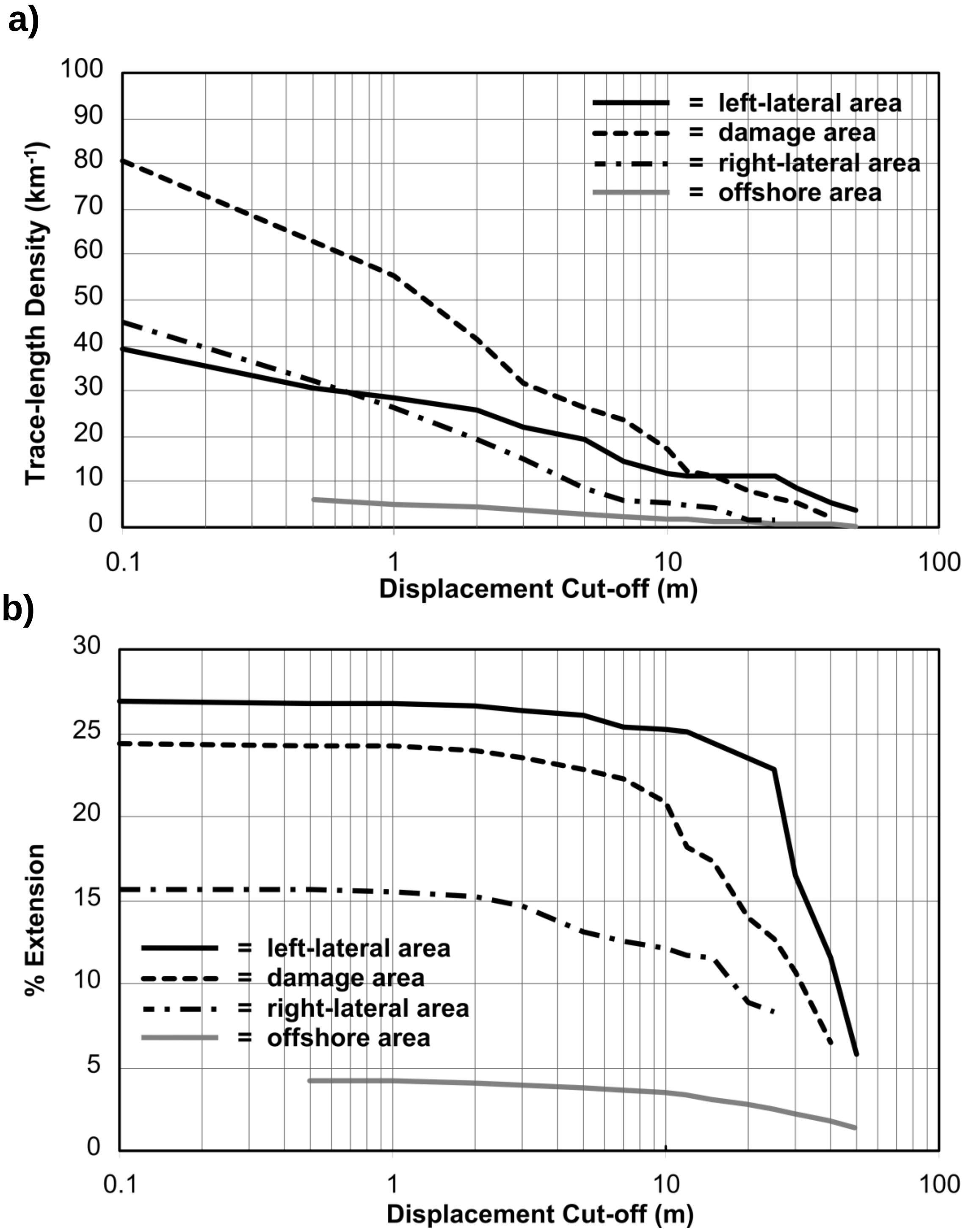
a)
100
90
80
70
60
50
40
30
20
10
0
Trace-length Density (km-1)
0.1
1
10
100
Displacement Cut-off (m)
= left-lateral area
= damage area
= right-lateral area
= offshore area
b)
30
25
20
15
10
5
0
% Extension
0.1
1
10
100
Displacement Cut-off (m)
= left-lateral area
= damage area
= right-lateral area
= offshore area

Figure

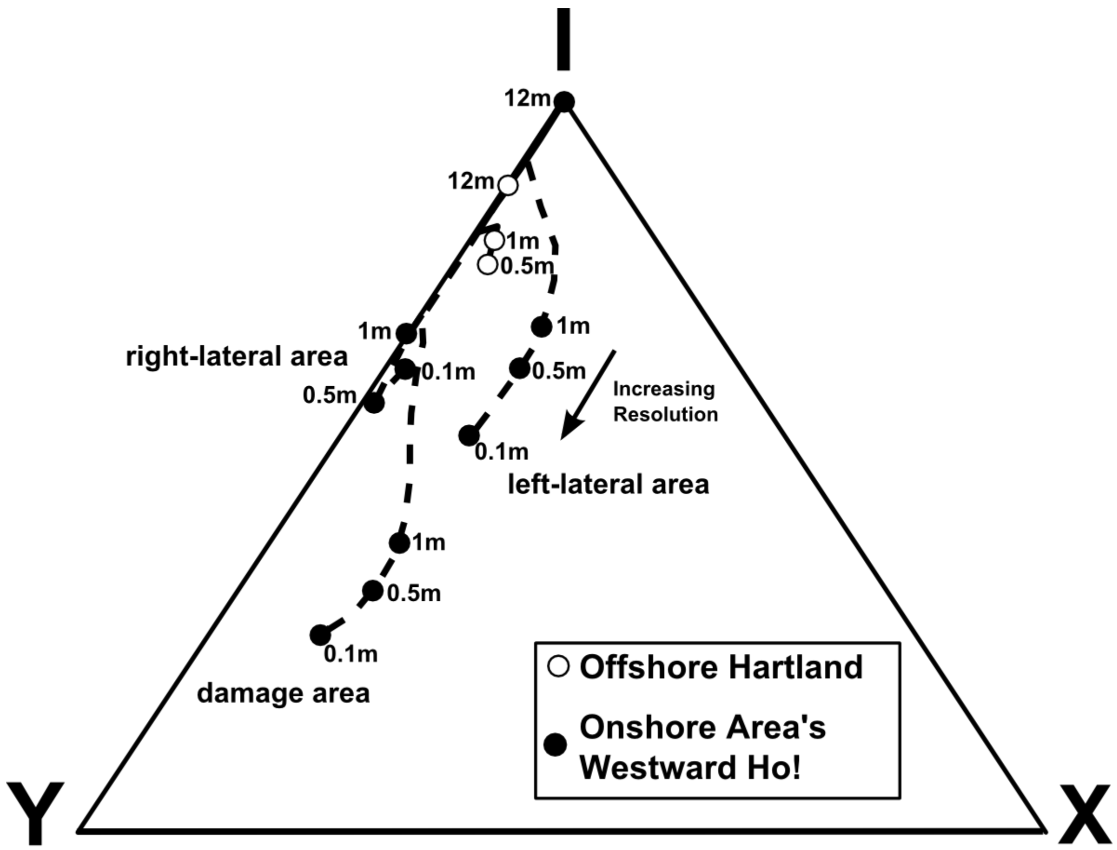
I
12m
12m
1m
0.5m
1m
1m
right-lateral area
0.1m
0.5m
0.5m
Increasing
Resolution
0.1m
left-lateral area
1m
0.5m
0.1m
damage area
Offshore Hartland
Onshore Area's
Westward Ho!
Y
X